Canadian Geotechnical Journal

Article

CPT-based design method for helical piles in sand

Eduardo Bittar[a], **Barry M. Lehane**[a], **Anthony Blake**[b], **David Richards**[b], **David White**[b], **Sam Mahdavi**[a], **and Benjamin Cerfontaine**[b]

[a]School of Engineering, The University of Western Australia, Australia; [b]Faculty of Engineering and Physical Sciences, University of Southampton, UK

Corresponding author: **Barry M. Lehane** (email: Barry.Lehane@uwa.edu.au)

Abstract

Helical piles are used extensively for low and medium rise developments and are a popular foundation solution in cases where resistance to significant uplift loads is required. The ability to re-use helical piles and recent interest in their use as foundations in offshore wind and solar energy applications has renewed interest in improving existing design methods. This paper presents the results from field investigations in medium dense and dense sand that examine effects on the axial tension and compression capacity of varying the helix pitch, shaft diameter, advancement ratio and shaft tip geometry. The results from the 20 pile tests conducted (many of which included instrumentation) indicate low sensitivity to a range of the investigated parameters and a strong correlation of the capacity to the cone penetration test resistance. A design method based on these findings is proposed for typical helical pile geometries and is shown to provide predictions that are generally within 10 to 15% of the axial capacities reported for 30 other well documented pile tests reported in the literature. The method, referred to as UWASP-22, incorporates a simple means of estimating the load-displacement response of a helical pile as well as a formulation enabling prediction of the installation torque which is a common quality control measure for helical piles.

Key words: helical pile, cone penetration test, sand, torque

1. Introduction

Helical (or screw) piles have been used in construction for over 200 years (Perko 2009) and, up to the turn of the century, have been largely employed as anchors and to provide uplift capacity (Q_t) and compression capacity (Q_{com}) for light and medium weight structures. Due to developments in torque motor capabilities (with capacities of up to 300 kNm), helical piles with shaft diameters as large as 600 mm and axial capacities more than 2500 kN are now being used for commercial and residential buildings, and to support heavy equipment in industrial plants (Elsawy et al. 2019; da Silva and Tsuha 2021). According to Spagnoli and de Hollando Cavalcanti (2020), larger single-helix piles are known by different names such as TSUBASA pile, NS-ECO pile and Steel Rotation Pile.

More recently, helical piles have been considered as an alternative solution for offshore foundations due to their large uplift capacity (Spagnoli and Gavin 2015) and minimal noise pollution during installation (Cerfontaine et al. 2021). The ability to reuse helical piles after their removal by reverse rotation adds to their attractiveness for use in floating or jacket-founded wind turbines or wave energy converters. However, the large loads applied in the offshore environment will demand significant enhancements to the helical pile geometries currently used onshore. For example, Davidson et al. (2020) showed in centrifuge tests that helical pile geometries capable of supporting a typical four-legged offshore jacket structure would require an installation torque (T) of 7 MNm, that is, more than 20 times greater than the typical torque machines used onshore. Research to address the installation challenges of offshore helical piles has been undertaken as part of the "EPSRC Supergen project" (EP/N006054/1 2016). A separate experimental component of the same research project presented in this paper examines factors affecting the installation resistance and axial capacity of helical piles in sand which can both assist extrapolation of findings to offshore conditions and improve current design methods for onshore helical piles.

The axial capacity of helical piles in sand is commonly estimated using conventional bearing capacity theory derived from anchor laboratory and field test results (e.g., Mitsch and Clemence 1985). These so-called "theoretical methods" are limited as they require estimation of appropriate soil strength parameters while capacity estimates are very sensitive to these parameters. As a consequence, there is a high practical reliance on the relationship between axial capacity and the torque applied during installation, where pile installation is continued to the depth at which the measured torque is considered sufficient to generate the required axial capacity according to that relationship. The most popular capacity-torque ($Q_t - T$) relationship is given as follows and was proposed by Perko (2009) from results on 239 test piles with typical shaft diameters (d) of between 50 mm and 250 mm and typical helix diameter (D_h) to shaft diameter ra-

tios (D_h/d) of between 2 and 4.

(1a) $Q_t = TK_t$

where

(1b) $K_t = 2.49/d^{0.92} inm^{-1}$

The coefficients of determination (R^2) for eq. 1a are 0.49 for compression piles and 0.71 for tension piles. These relatively low values reflect limitations in the assumption of a direct unique relationship between Q_t and T and may also be associated with poor quality installation torque measurements obtained using hydraulic pressure torque indicators (Harnish 2015). Both the magnitude of the required installation torque (T) and the pile capacity (Q_t) can be attributed directly to the soil shearing resistance of the embedded pile area comprising the shaft and helices. There is, however, limited information quantifying the relative contribution of the resistance provided by the helices and shaft. Centrifuge tests reported by Brown (2019) indicate that the magnitude of the installation torque is controlled primarily by the shaft surface area although other authors such as Tsuha and Aoki (2010) and da Silva and Tsuha (2021) suggest that the torque is largely controlled by the surface area of the helices. Expressions such as eq. 1 are widely used in the helical pile industry for both quality control and quality assurance.

Given the limitations of $Q_t - T$ correlations and the fact that the application of these correlations does not allow capacity assessments to be made in advance of site works, it is clear that a design method that has greater reliability than the published theoretical methods mentioned above is required (Fateh et al. 2017). The widespread successful application of cone penetration test (CPT) based methods for other pile types prompted the investigation described in this paper into the potential of another CPT method for prediction of axial pile capacity. To assist with this investigation, a field testing programme, involving 20 helical piles, was performed to examine the influence of a range of pile configuration and installation parameters on capacity in medium dense and dense sand. This study and its findings are described and then applied to a new database of static load tests leading to a proposed set of simple formulations that allow the load displacement characteristic of a helical pile to be estimated. The proposed method is shown to predict axial capacities and installation torques to an accuracy considerably better than other popular existing approaches (Bittar et al. 2022).

2. Helical pile parameters investigated

The field investigation described in this paper was devised to examine the influence of the following parameters on the installation resistance and the static axial capacity of helical piles.

- Advancement ratio (AR), defined as the ratio of the vertical displacement for one rotation (Δz_h) to the helix pitch (p).
- Axial thrust (often referred to as "crowd") applied during installation.
- Helix pitch (p).
- Loading direction (tension and compression).
- Configuration at shaft base (open, closed, tapered).
- Number of helices (single/double).

Insights from previous investigations into the influence of these parameters are summarised in the following.

2.1. Advancement ratio and axial thrust

The AR of a helical pile is intimately related to the axial thrust applied during installation. The axial thrust is rarely monitored during installation and operators usually apply an initial thrust until the helix "bites" the sand, after which the continued rotation is normally sufficient to pull the pile into the ground without application of additional thrust. The rotation rate of a helical pile typically varies between 5 and 30 revolutions per minute.

Bradshaw et al. (2018) suggest that an AR value of about 0.5 is achieved under these normal operating conditions. As such, the helical pile is "over-flighting" and potentially loosening sand below the helix and densifying sand above the helix. Such over-flighting can be reduced by applying a thrust to the pile which increases AR and the pull-down tension applied by the helix. A "pitch matched" condition occurs at $AR = 1$ when the helix advances by one helix pitch for each helix revolution with no disturbance. Sharif et al. (2021*a*) showed that significantly higher thrusts are required to achieve $AR = 1$ while the thrust had little effect on the installation torque. Cerfontaine et al. (2021) show in centrifuge tests that AR influences the in-service performance of the helical pile, with improved tensile capacity when $AR < 0.8$ and improved compression capacity for $AR > 0.8$.

2.2. Helix pitch (p)

The geometric pitch of onshore helical piles is rarely varied and is typically set at 3 inches (76.2 mm) (Perko 2009; ICC-ES 2017). Using three-dimensional discrete-element modelling (DEM) Sharif et al. (2021*a*) concluded that, for piles with $AR \sim 0.95$ and p values between 75 and 150 mm, a greater helix pitch increases tension capacity while a smaller pitch increases compression capacity. The same analyses showed that the helix pitch has no impact on the installation requirements at $AR = 0.95$ but the required installation force reduced as AR reduces. However, Lutenegger (2013) concluded from field tests that the installation torque or tension capacity do not vary systematically with p, although observations may have been affected by in-situ variability of the sand.

2.3. Loading direction

Zhang (1999) compiled a database of helical piles tests, many of which were conducted by Trofimendkov and Mariupolskii (1965). The database comprised tension and compression tests on about 200 piles with helix diameters (D_h) ranging from 0.45 to 1.0 m and embedded to depths of up to 7 m. Capacity was defined at a pile head displacement of 10% of the helix diameter. It was concluded that ultimate compressive capacity is, on average, 1.3 times more than the ultimate tensile capacity. Perko (2009) observed that the tensile capacity of helical piles measured at three sites was be-

tween 16% and 33% less than the measured compression capacity. DEM analyses presented by Sharif et al. (2020) suggest a larger dependence on loading direction with predicted ratios of compression to tension capacity of as high as 3 in medium dense and dense sand. These analyses appear to show a greater influence of the proximity of the free surface on the uplift capacity than observed in the field.

2.4. Configuration at shaft base (open, closed and tapered)

Using DEM, Sharif et al. (2021*b*) concluded that modifying the geometry at the base of a helical pile can reduce the required compressive installation force by up to 50%. Cerfontaine et al. (2021) also observed in centrifuge tests that an asymmetric tip geometry (cut at 45° to the horizontal) can reduce the required installation axial thrust. However, both sets of analyses indicated that the shaft base condition had no influence on the uplift capacity and little effect on the compression capacity.

2.5. Number and spacing of helices

When helical piles have more than one helix, the failure mechanism can involve either individual bearing failures around each helix or shear failure on a cylindrical surface with the same diameter as the helices. Rao et al. (1991), Lutenegger (2009) and others, conclude that the cylindrical failure mechanism can occur in sand when s/D_h is less than between 1.5 and 2.25 (where s is the spacing between helices). However, Alwalan and El Naggar (2021) argue that other factors such as soil strength and pile displacement affect the s/D_h ratio at which the cylindrical mechanism transitions to the individual mechanism. In practice, most manufacturers design helical piles with multiple helices employing s/D_h ratios in excess of about 3 (Perko 2009).

3. Experimental programme

3.1. Site conditions and test pile details

The majority of field testing for the current study involved monitored installation and load testing of 18 helical piles installed in a siliceous sand site located at Shenton Park, which is a field station research site operated by The University of Western Australia (UWA). The site has been previously characterised using in situ and laboratory tests (Lehane et al. 2004; Schneider et al. 2008) and employed for field testing of retaining walls and driven piles in sand (Li and Lehane 2010; Bittar et al. 2020). The helical piles in Shenton Park were installed and tested in four phases (P1, P2, P3 and P4) at different periods during 2019 and 2020. Test pile and CPT locations are shown in Fig. 1*a* and 1*c* and one resistance (q_c) profiles are shown on Fig. 1*b*. The q_c value is typically 5–10 MPa in the upper 1 m and about 5 MPa below this depth. Based on site specific correlations with q_c (Lehane et al. 2004), the relative density (D_r) along the embedded pile lengths was assesssed to vary between 0.50 and 0.68.

The piles tested in Shenton Park were mild steel tubes, which were sandblasted to a centerline average roughness of about 10 μm. Eight pile configurations were tested and, as shown in Fig. 2, all piles had the same helix diameter (D_h = 384 mm) but employed two different shaft diameters (d) of 114.3 mm and 139.7 mm and two different helix pitches (p) of 100 and 200 mm. The piles were installed to depths (L) of between 2.6 and 2.8 m, giving a L/D_h ratio of 7. Piles were generally extracted and re-used after static load testing. Different base configurations involving flat and asymmetric tips (cut at an angle of 45° to the horizontal direction) were used and these were either open or closed-ended, as shown in Fig. 2. One pile had a double helix with a s/D_h ratio of 2. The ratio with the helix diameter of the distance from the pile tip to the mid-height of the base helix (h/D_h) ranged from 0.31 to 0.74. The configurations of all helical piles are generally consistent with those used in practice.

As shown in Fig. 2, strain gauges to monitor both torque and axial load were installed immediately above the helix in five of the eight piles to measure the contributions of the helix and the shaft to the installation resistance and axial capacity. Details of the instrumentation design and calibration are provided by Blake et al. (2023).

To extend the study to longer helical piles in denser sand, two additional piles (L = 5 m, d = 114.3 mm, D_h = 384 mm and asymmetric closed end tip) were installed and tested in 2021 at another site located in Bayswater, Western Australia. The soil at this site comprises medium uniform sand with an average CPT q_c value of 10–15 MPa along the embedded pile length. The q_c profile and configuration of the test piles are shown in Fig. 3.

3.2. Installation monitoring and load testing

The applied torque (T), thrust (V) and angular rotation (θ) were measured at the pile head during installation using a ProDig Intelli Tork® measurement system (model C441-S400 Wi-Fi—S/N 119637). The instrument measured torque and thrust using in-built strain gauged load cells and measured rotation with magnetometers. The rated maximum T and V values of the instrument are 81 kNm and 4.4 MN respectively. Measured data were transmitted in real time via an on-board 2.4 GHz wireless transmitter to the Intelli-Tork® App operating on an Android Smartphone. Verification of the calibration of the Torque and Thrust sensors within the Intelli Tork device was performed in the structures laboratory at UWA.

The piles were installed using a torque head supported by an excavator machine. For most of the test piles, installation was controlled to achieve minimum possible thrust and a rotation rate (ω) of 5 revolutions per minute (rpm). One pile at Shenton Park and another at Bayswater were installed with target constant V values of 50 kN during the complete installation to investigate the effect of thrust on the installation torque and axial capacity.

The static load tests were conducted typically 4 to 8 days after the pile installation. Compression tests were performed using the reaction provided by a 25 tonne CPT truck and tension tests employed a testing frame founded on strip footings located about 1.5 m away from the test piles. The set-ups employed for the compression and tension tests have been employed previously by Xu (2007), Lim (2013) and Bittar et al.

Fig. 1. Helical piles installed in Shenton Park and CPT data. CPT = cone penetration test.

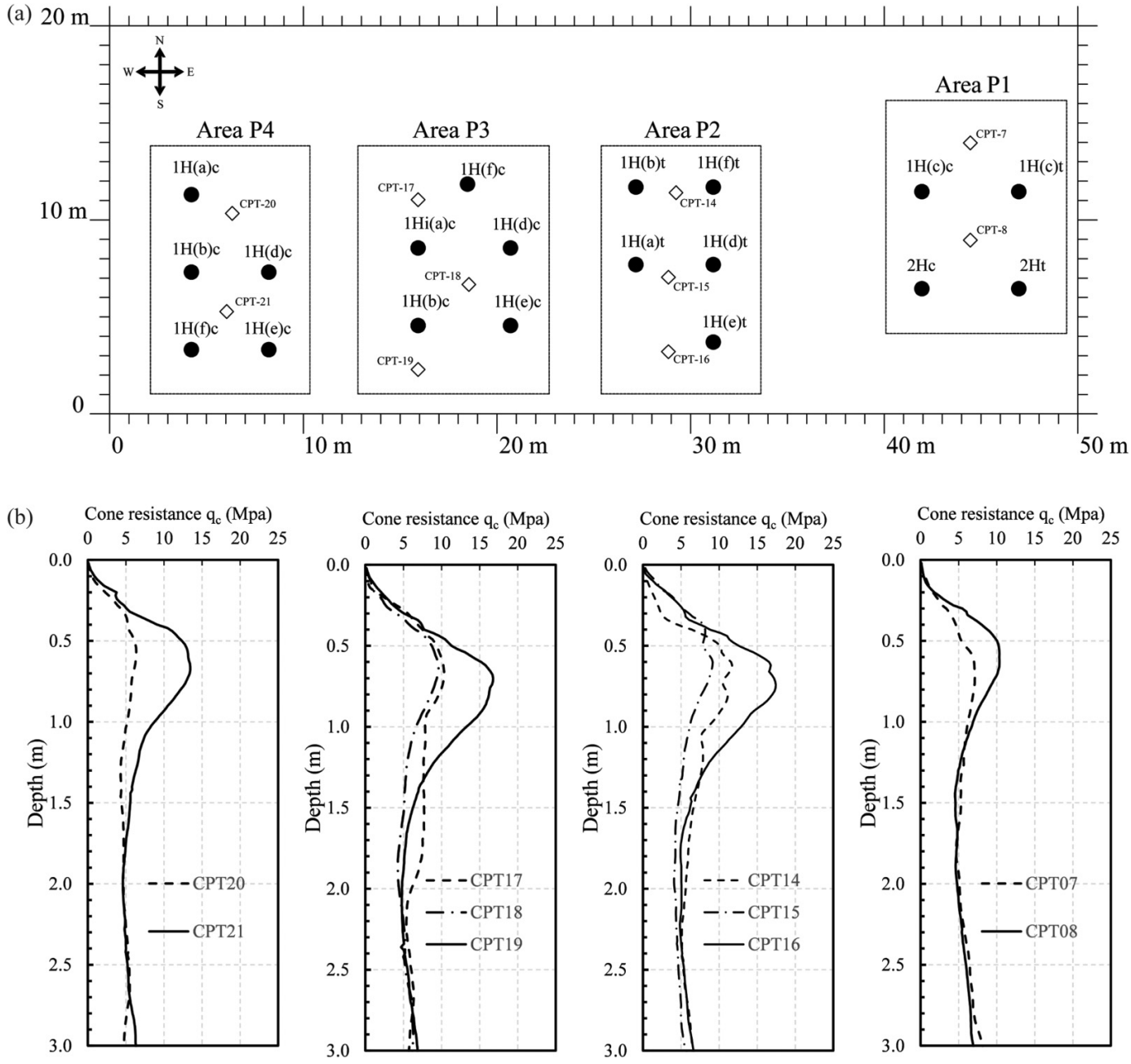

(2020) for tests on driven piles and are described in full in these references.

The axial load was applied in increments of between 5% and 10% of the anticipated axial capacity using an electric pump connected to a hydraulic jack reacting against either the CPT truck or tension testing frame. Pause periods during each load increment were typically about 10 mins in duration and creep displacements of the piles were negligible before application of the subsequent increment. The load was measured at the pile head and recorded by a digital load cell and verified by a pressure gauge connected to the calibrated hydraulic jack. The pile head displacements were measured using two linear variable differential transformers mounted on an independent reference beam.

4. Experimental results

4.1. Pile installation

A full description and interpretation of the measurements obtained during installation of the test piles is provided in Blake et al. (2023). Details relevant to the factors potentially influencing axial capacity are summarized in Tables 1 and 2 for piles subjected to tension and compression tests respectively. These tables list the pile geometry specifics (L, h, d, D_h, p), the CPT closest to the test pile, the average thrust (V) and torque (T) applied over the final penetration distance of 1 D_h during installation, the average rotation rate (ω), vertical velocity (v) and AR.

Fig. 2. Configuration of Shenton Park test piles.

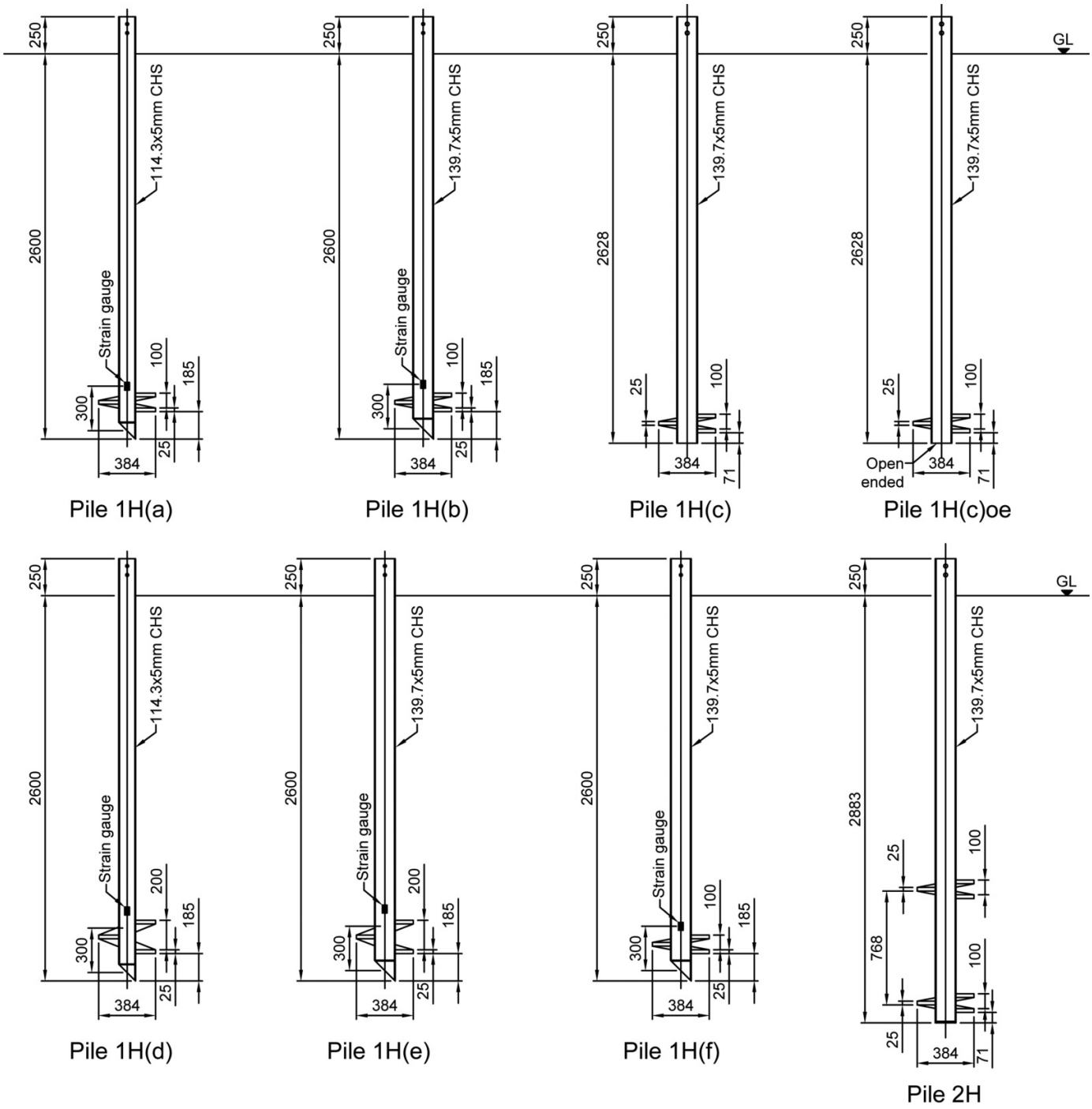

Example data from three pile installations are presented in Fig. 3 and highlight a number of features common to all installations:

(i) The installation torque does not show a one-to-one correspondence with the CPT q_c
(ii) *AR* is variable despite *V* and ω being relatively constant.
(iii) Increasing V increases *AR*; see Fig. 3*a* and 3*b*. Further independent tests showed higher *AR* values are achievable at higher rotation rates.
(iv) Higher *T* values are required in the denser sand at Bayswater (see Fig. 3*a* and 3*c*).

4.2. Pile axial capacity (single helix)

Tables 3 and 4 summarise the pile capacities, measured at a pile head displacement (δ) of 0.1 D_h, in the 9 tension tests and 11 compression tests conducted on single helix piles for this study. For strain gauged piles, the tables also list the contribution of the shaft above the level the gauges to

Fig. 3. Typical installation monitoring for (*a*) pile 1 H(b) with $p = 0.1$ m, (*b*) pile 1 H(f) with high thrust applied and (*c*) pile 1 H(g) at Bayswater site.

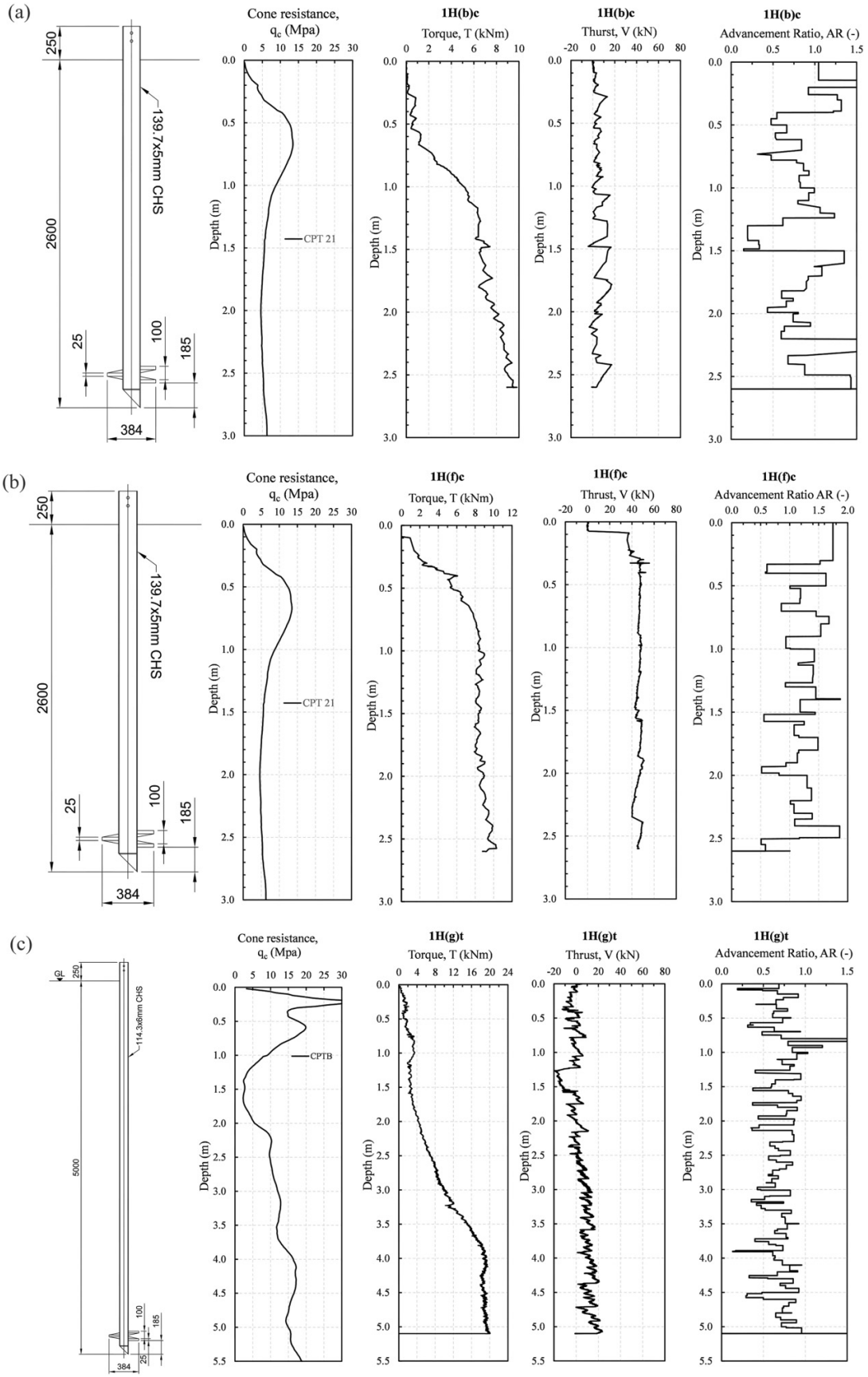

Table 1. Installation characteristics of helical piles tested in tension at Shenton Park and Bayswater.

N	Pile name	CPT	Site	L (m)	d (m)	D (m)	p (m)	V (kN)	T (kNm)	ω (rpm)	v (mm/s)	AR
1	1 H(c)oe	CPT08	Shenton Park	2.7	0.1397	0.385	0.1	1.3	10.7	5.5	5.2	0.61
2	1 H(c)	CPT07	Shenton Park	2.7	0.1397	0.385	0.1	0.9	10.7	4.6	3.7	0.56
3	1 H(b)	CPT14	Shenton Park	2.6	0.1397	0.385	0.1	3.9	8.0	3.8	5.0	0.72
4	1 H(e)	CPT16	Shenton Park	2.6	0.1397	0.385	0.2	4.3	8.7	4.3	8.2	0.60
5	1 H(a)	CPT15	Shenton Park	2.6	0.1143	0.385	0.1	6.5	5.2	5.0	6.7	0.81
6	1 H(d)	CPT15	Shenton Park	2.6	0.1143	0.385	0.2	1.0	6.2	4.9	10.0	0.65
7	1 H(f)	CPT14	Shenton Park	2.6	0.1397	0.385	0.1	6.3	8.5	4.9	7.2	0.94
8	1 H(g)	CPTB	Bayswater	5.0	0.1143	0.385	0.1	5.7	19.5	3.8	4.0	0.69
9	1 H(h)	CPTB	Bayswater	5.0	0.1143	0.385	0.1	56.0	21.0	3.9	4.9	0.82

Note: AR = advancement ratio; CPT = cone penetration test.

Table 2. Installation characteristics of tested helical piles in compression at Shenton Park.

N	Pile Name	CPT	Site	L (m)	d (m)	D (m)	p (m)	V (kN)	T (kNm)	ω (rpm)	v (mm/s)	AR
10	1 H(c)	CPT07	Shenton Park	2.7	0.1397	0.385	0.1	1.4	9.50	4.8	3.5	0.50
11	1 H(a)	CPT18	Shenton Park	2.6	0.1143	0.385	0.1	−1.4	6.50	5.3	6.3	0.80
12	1 H(b)	CPT19	Shenton Park	2.6	0.1397	0.385	0.1	−2.85	8.80	4.6	5.7	0.79
13	1 H(e)	CPT18	Shenton Park	2.6	0.1397	0.385	0.2	0.59	9.50	5.4	10	0.60
14	1 H(d)	CPT18	Shenton Park	2.6	0.1143	0.385	0.2	−0.8	7.80	4.1	9	0.65
15	1 H(f)	CPT17	Shenton Park	2.6	0.1397	0.385	0.1	−7.5	8.95	5.4	6.5	0.78
16	1 H(a)	CPT20	Shenton Park	2.6	0.1143	0.385	0.1	4.2	6.50	4	5.2	0.82
17	1 H(b)	CPT21	Shenton Park	2.6	0.1397	0.385	0.1	4.4	10.00	5.3	6.1	0.80
18	1 H(d)	CPT21	Shenton Park	2.6	0.1143	0.385	0.2	3.1	8.50	4.30	7.70	0.60
19	1 H(e)	CPT21	Shenton Park	2.6	0.1397	0.385	0.2	0.63	11.50	4.5	8.5	0.59
20	1 H(f)	CPT21	Shenton Park	2.6	0.1397	0.385	0.1	44.0	10.00	4.7	8	1.20

Note: AR = advancement ratio; CPT = cone penetration test.

Table 3. Shaft, helix and total pile capacity (at $\delta = D_h/10$) for helical piles tested in tension at Shenton Park and Bayswater.

No	Pile name	CPT	L (m)	D (m)	D_h (m)	p (m)	AR	$Q_{shaft,\,c}$ (kN)	$Q_{h,\,c}$ (kN)	$Q_{ult,\,c}$ (kN)	$Q_{shaft,\,m}$ (kN)	$Q_{h,\,m}$ (kN)	$Q_{ult,\,m}$ (kN)	$Q_{ult,\,m}/Q_{ult,\,c}$
1	1 H(c)oe	CPT08	2.7	0.14	0.385	0.1	0.61	28.6	103.7	132.3	NM	NM	138	1.04
2	1 H(c)	CPT07	2.7	0.14	0.385	0.1	0.56	25.7	116.1	141.8	NM	NM	148	1.04
3	1 H(b)	CPT14	2.6	0.14	0.385	0.1	0.72	30.2	91.4	121.5	25	106	131.4	1.08
4	1 H(e)	CPT16	2.6	0.14	0.385	0.2	0.6	37.1	90.5	127.6	30	107	137	1.07
5	1 H(a)	CPT15	2.6	0.11	0.385	0.1	0.81	20.1	80.1	100.2	NM	NM	106	1.06
6	1 H(d)	CPT15	2.6	0.11	0.385	0.2	0.65	20.1	80.1	100.2	23.7	82.1	105.8	1.06
7	1 H(f)	CPT14	2.6	0.14	0.385	0.1	0.94	30.2	91.4	121.5	29	98	127	1.04
8	1 H(g)	CPTB	5	0.11	0.385	0.1	0.69	86.7	263	349.8	NM	NM	400	1.14
9	1 H(h)*	CPTB	5	0.11	0.385	0.1	0.82	86.7	263	349.8	NM	NM	325	(0.93)
NM	Not measured												**μ**	1.07
*	High thrust (not considered in μ and CoV determination)												**CoV**	0.05

Note: AR = advancement ratio; CoV = coefficient of variation; CPT = cone penetration test.

the capacity ($Q_{shaft,\,m}$) and that of the helix, shaft and tip below this location ($Q_{h,\,m}$). Typical variations of axial load with displacement (discussed later) are provided in Fig. 7 and reveal a ductile response under both compression and tension loading.

The axial capacities of the single helix piles at Shenton Park are plotted against various parameters on Fig. 4. All of these piles have the same helix diameter (0.384 mm) and length (2.65 ± 0.05 m). A clear trend for capacities in compression to be higher than in tension is evident while the dependence on other parameters appears small. There is a modest tendency for capacity to increase with larger shaft diameters (d). The helix pitch (p) does not have a large influence on capacity and the data do not reveal any significant effect of the pile tip geometry. The compression capacities of the longer piles at Bayswater are over double those at Shenton Park, which is consistent with difference in q_c values at both sites.

Table 4. Shaft, helix and total pile capacity for helical piles tested in compression at Shenton Park.

No	Pile name	CPT	L	d	D_h	p	AR	$Q_{shaft,\,c}$	$Q_{h,\,c}$	$Q_{ult,c}$	$Q_{shaft,\,m}$	$Q_{h,\,m}$	$Q_{ult,\,m}$	$Q_{ult,\,m}/Q_{ult,\,c}$
–	–	–	m	m	m	m	–	kN	kN	kN	kN	kN	kN	–
10	1 H(c)	CPT07	2.7	0.1397	0.385	0.1	0.50	27.0	149.5	176.5	NM	NM	187	1.06
11	1 H(a)	CPT18	2.6	0.1143	0.385	0.1	0.80	22.2	122.1	144.2	NM	NM	134	0.93
12	1 H(b)	CPT19	2.6	0.1397	0.385	0.1	0.79	38.5	122.1	160.6	30	146	176	1.1
13	1 H(e)	CPT18	2.6	0.1397	0.385	0.2	0.60	27.1	122.1	149.2	NM	NM	142	0.95
14	1 H(d)	CPT18	2.6	0.1143	0.385	0.2	0.65	22.2	120.5	142.7	NM	NM	154	1.08
15	1 H(f)	CPT17	2.6	0.1397	0.385	0.1	0.78	33.9	133.1	166.9	25	135	160	0.96
16	1 H(a)	CPT20	2.6	0.1143	0.385	0.1	0.82	19.0	121	140.0	24	126	150	1.07
17	1 H(b)	CPT21	2.6	0.1397	0.385	0.1	0.80	33.1	116.8	149.9	NM	NM	163	1.09
18	1 H(d)	CPT21	2.6	0.1143	0.385	0.2	0.60	27.1	116.8	143.9	22	130	152	1.06
19	1 H(e)	CPT21	2.6	0.1397	0.385	0.2	0.59	33.1	116.8	149.9	NM	NM	170	1.13
20	1 H(f)∗	CPT21	2.6	0.1397	0.385	0.2	1.20	33.1	116.8	149.9	21	173	194	– 1.29
NM	Not measured												μ	1.04
∗	High thrust (not considered in μ and CoV determination)												**CoV**	0.06

Note: AR = advancement ratio; CoV = coefficient of variation; CPT = cone penetration test.

Fig. 4. Axial capacities measured at Shenton Park and Bayswater on single helix piles with $L/D_h = 7$ and $D_h = 0.384$ m (pile numbers indicated on the figure correspond with those in Tables 1 and 2).

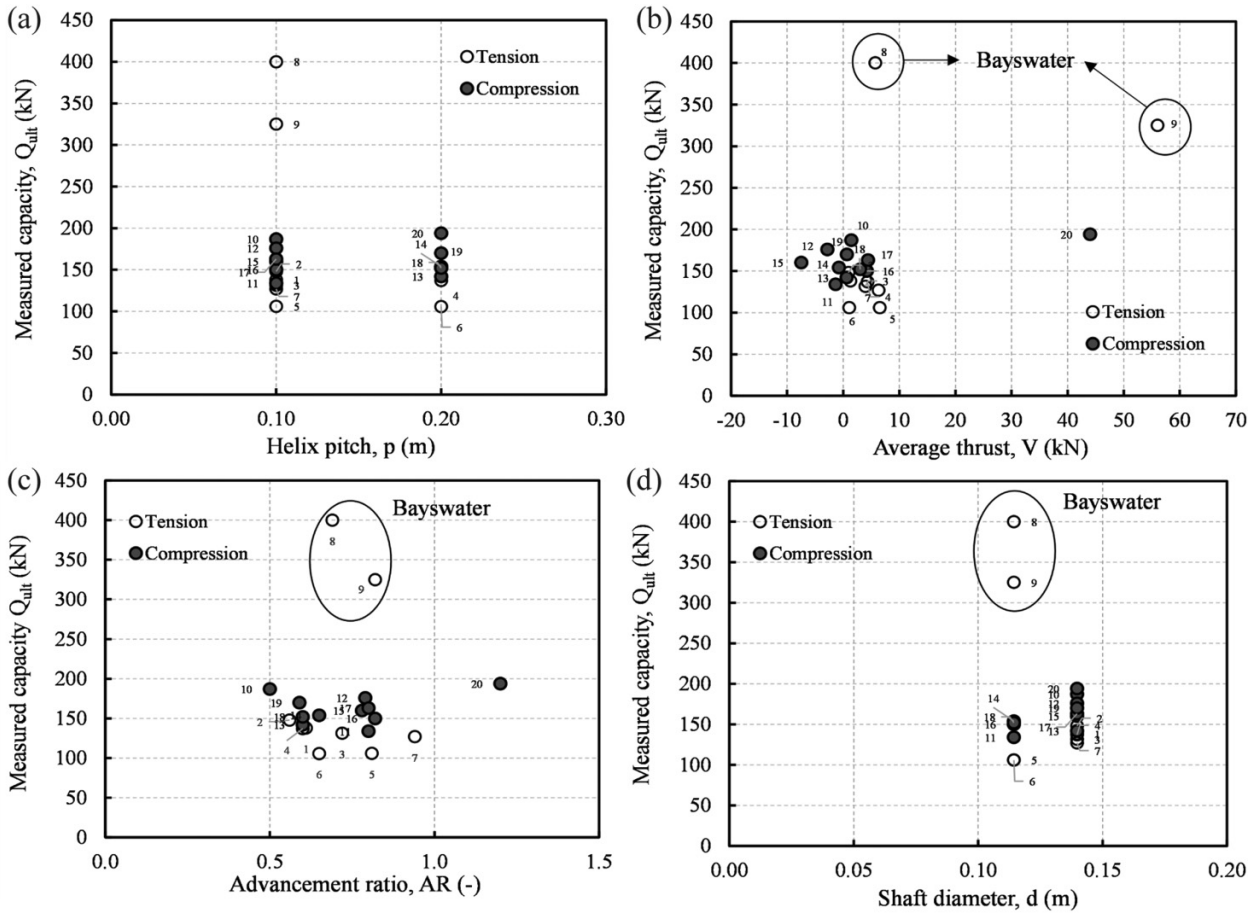

In general, the observed effects of helical pile parameters are consistent with those discussed previously. For example, the increase in AR from 0.59 to 1.2 at Shenton Park, arising from a greater applied thrust, led to a 14% increase in compressive capacity which is similar to the increase observed in centrifuge tests reported by Cerfontaine et al. (2021). Reduced tension capacity for the pile in Bayswater that was subjected to a high installation thrust is also consistent with tests of Cerfontaine et al. (2021), as is the low sensitivity of capacity to the geometry of the helical pile tip.

Fig. 5. Measured helix and shaft capacity contribution for pile No. 15 in Shenton Park (see Table 4) and pile No. 32 in Blessington (see Table 5).

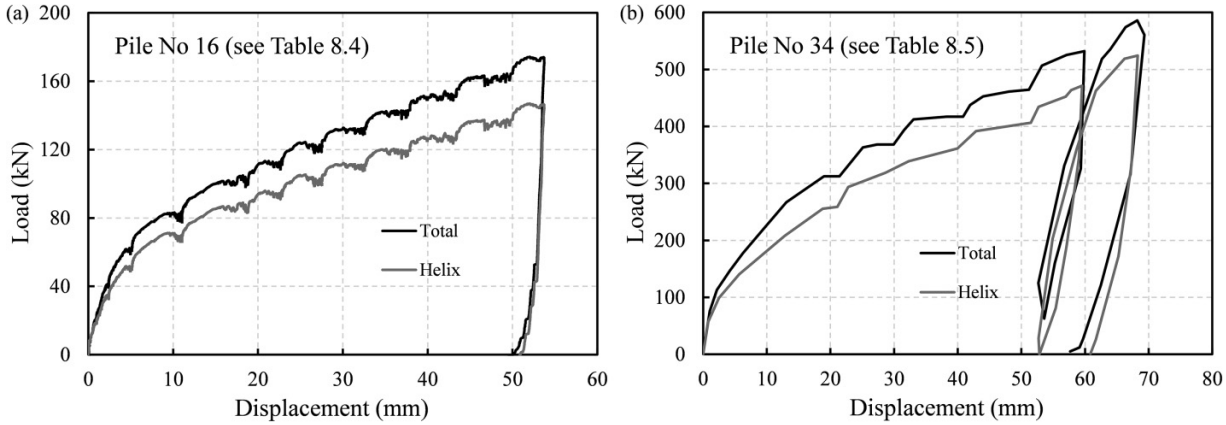

4.3. Contribution of helix and shaft to capacity

As seen in Tables 3 and 4, the shaft resistance in compression and tension of the single helix piles at Shenton Park was typically 25 kN and contributed between 18% and 27% of the total compression and tension capacities respectively. The shaft resistance provided the majority of the axial resistance up to a displacement of about 1.5 mm (when the shaft capacity was fully developed) after which the helix provides all of the resistance. A typical example of the development of axial resistance contributed by (and below) the helix, compared with the overall resistance, is provided on Fig. 5*a* for a pile tested in compression. This trend is closely comparable to that shown in Fig. 5*b* which was recorded Gavin et al. (2014) for a compression test on a helical piles with a similar configuration in very dense sand.

5. Prediction of axial capacity using the CPT

The field testing programme indicated a relatively low sensitivity of axial capacity to a range of parameters. Although variability between the pile configurations and in the respective q_c profiles at each test pile location could mask small effects of these parameters, a reasonable starting point for derivation of a design method is to assume tension and compression capacities differ (as clearly observed) and that the capacity of helical piles with typical geometries and installation parameters comprises a shaft and a helix component of resistance which vary with the CPT q_c value. Typical helical piles in current use have d/D_h values in the range 0.25 to 0.5, $L/D_h > 5$, $s/D_h \geq 2$, $AR \leq 0.8$ and $0.075\text{ m} < p < 0.2\text{ m}$ (Tappenden 2007; Perko 2009; Sakr 2012; Davidson et al. 2020). The proportional relationship between shaft friction (q_s) and q_c observed for bored piles in sand (Bustamante and Gianeselli 1982; Doan and Lehane 2021) provides a precedent for this assumption for helical piles while the proportional relationship between bearing pressure and q_c for footings on sand (e.g., Mayne 2014; Liu et al. 2020) supports the proposal to link the helix resistance to q_c.

Relationships for shaft friction (q_s) and helix bearing resistance at a displacement of $0.1D_h$ ($q_{b0.1}$) can therefore be expressed as follows, where β_c and $\alpha_{b0.1}$ are empirical factors:

$$q_s = q_c/\beta_c \quad (2)$$

$$q_{b0.1} = \alpha_{b0.1} q_{c,avg} \quad (3)$$

To allow for variable q_c profiles in a similar way to that employed in footing design, $q_{c,avg}$ is taken as the average q_c in a zone extending a distance of D_h above and below the helix. A distance of 1 D_h is consistent with the zone of influence beneath a small footing on sand recommended by Burland and Burbidge (1985). For simplicity (and noting that higher tension capacities were measured in piles with large shaft diameters, d), the following expression is assumed in the derivation of the axial capacity of a single helix (Q_h) in both compression and tension:

$$Q_h = q_{b0.1} \pi D_h^2/4 \quad (4)$$

Shaft friction is calculated by integrating the shaft friction components over the shaft area above the uppermost helix. The total capacity is then obtained by summing the shaft and helix capacity. Based on available evidence discussed above, it is initially assumed here that interaction between helices is negligible when $s/D_h \geq 2$ and the contribution of the helices can be summed to obtain their total capacity. The contribution of shaft friction to the overall axial capacity of a helical pile is small (e.g., see Fig. 5) and therefore shaft friction below the base helix and in between helices is ignored.

The EXCEL© Tool *Solver* was applied to the load test data summarized on Tables 3 and 4 to derive best-fitting β_c and $\alpha_{b0.1}$ values for tension and compression tests (employing the CPT closest to each pile test). The analysis searched for values that gave a mean ratio of measured to calculated total capacity (μ) for the datasets close to unity with a minimum coefficient of variation (CoV) while ensuring that the ratios of the measured to calculated shaft capacities were also about unity. Test Nos. 9 and 20 were discounted from the statistical analyses as they were installed with a high thrust and were therefore atypical.

Fig. 6. Dependence of ratio of measured to calculated tension capacities ($Q_{t,m}/Q_{t,c}$) on AR for centrifuge piles reported by Cerfontaine et al. (2021). AR = advancement ratio.

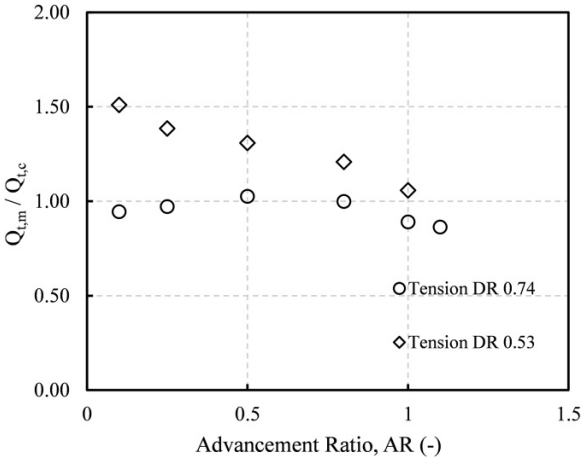

This statistical analysis indicated that capacities calculated with $\beta_c = 230$ and $\alpha_{b0.1} = 0.15$ for tension ($\alpha_{b0.1,t}$) and 0.20 for compression ($\alpha_{b0.1,c}$) provided the best overall fit to the data. Tables 5 and 6 compare the measured capacity (Q_m) and calculated capacity (Q_c) for each pile and confirm the suitability of the approach showing that, on average, Q_m/Q_c values are 1.07 and 1.04 in tension and compression respectively. The *CoV* is only 5 to 6% for both data sets indicating a low level of uncertainty for the approach for the test piles at the two sites investigated.

The β_c factor of 230 is close to the value of 175 (in compression) and 220 (in tension) recommended for bored piles in sand by Doan and Lehane (2021). Insufficient data exist to assess a directional dependence of β_c and adoption of a single value is considered sufficient given that the shaft typically contributes less than 20% to the overall resistance (e.g., see Fig. 5). The $\alpha_{b0.1}$ factor is also in good agreement with the value observed for footings and at the base of bored piles at a displacement of 10% of the foundation diameter (e.g., Lehane 2012; Mayne and Woeller 2014). This consistency emerges, as discussed by (Lehane 2019), because of the hemispherical expansion type mechanism of footings at this level of displacement and the proportional relationship between q_c and cavity expansion limit pressure.

5.1. Performance of prediction method against a database of single helix helical piles

To assess the general applicability of the expressions derived for the Shenton Park and Bayswater piles, a database of static load tests on single-helix helical piles was compiled from the literature and from tests shared with the authors by "Screw Piling Australia Pty Ltd." This database, which is summarised in Table 5, comprises 23 pile tests with 9 tests in tension and 14 in compression; the shafts of all piles were open-ended and the L/D_h ratios ranged from 6.4 to 13.3. The documented cases provided by "Screw Piling Australia" comprised piles that were typically loaded to a displacement of about 5% of D_h. The measured load displacement curves were therefore extrapolated using Chin's method (Chin 1970) to determine the capacity, defined at $0.1D_h$ (which was typically 15% higher than the measured load at a displacement of $0.05D_h$).

CPT q_c profiles were available at all test sites and were digitised to enable automated capacity calculations; these calculations adopted the same $\alpha_{b0.1}$ and β_c values derived for the Shenton Park and Bayswater tests. Measured and calculated capacities for the 23 pile tests are provided in Table 5 which shows that the mean (μ) ratio of measured to calculated capacity for this collection of tests is 0.92 and the *CoV* of these ratios is only 0.09 (noting that comparable *CoVs* for other CPT pile design methods are typically greater than 0.3, Phoon and Retief 2016).

5.2. Performance of prediction method in centrifuge tests

Much recent research on helical piles has been conducted in the centrifuge and it is therefore of interest to compare the calculation approach outlined above with the capacities of 11 single helix piles with $L/D_h = 7.2$ tested in tension, reported by Cerfontaine et al. (2021). The piles were installed at a constant rotation rate of 3 rpm but the thrust load (V) was varied to assess the effect of the *AR* on axial capacity. The reported q_c profiles were corrected for shallow penetration effects according to the procedure of Lehane et al. (2022).

The ratios of measured to calculated capacity are plotted on Fig. 6 for the two relative densities (D_r) investigated. It is evident that the predictions for the tension capacities in the sand with $D_r = 0.74$ match the measured capacities almost perfectly over the wide range of *AR* values investigated. The measured capacities in the looser sand are up to 25% higher at low AR values less than 0.5, which is not typical of field scale helical piles.

5.3. Performance of prediction method for helical piles with multiple helices

The performance of the calculation method was investigated for helical piles with two helices. Two double helix helical piles were installed in Shenton Park (one tested in tension and one in compression) as part of this study, and five test piles with adjacent CPT q_c data were sourced from the literature. The characteristics of these piles as well as their measured and calculated axial capacities are presented in Table 6. The calculation assumed no interaction between the helices even though two of the six piles had a s/D_h ratio of only 1.5.

The μ and *CoV* values of ratios of measured to calculated for this dataset of 0.97 and 0.13, respectively, indicate that the calculation approach works well and suggests that interaction between the helices is not significant.

6. Load displacement prediction

The comparable $\alpha_{b0.1}$ values established for footings and the helix of helical piles suggests that a CPT-based approach similar to that proposed for prediction of the load-displacement response of footings in sand (Mayne 2014; Lehane 2019) may also be applied to helical piles. This approach suggests that the bearing pressure on a helix normal-

Fig. 7. Measured and calculated load–displacement response of typical helical piles in the database.

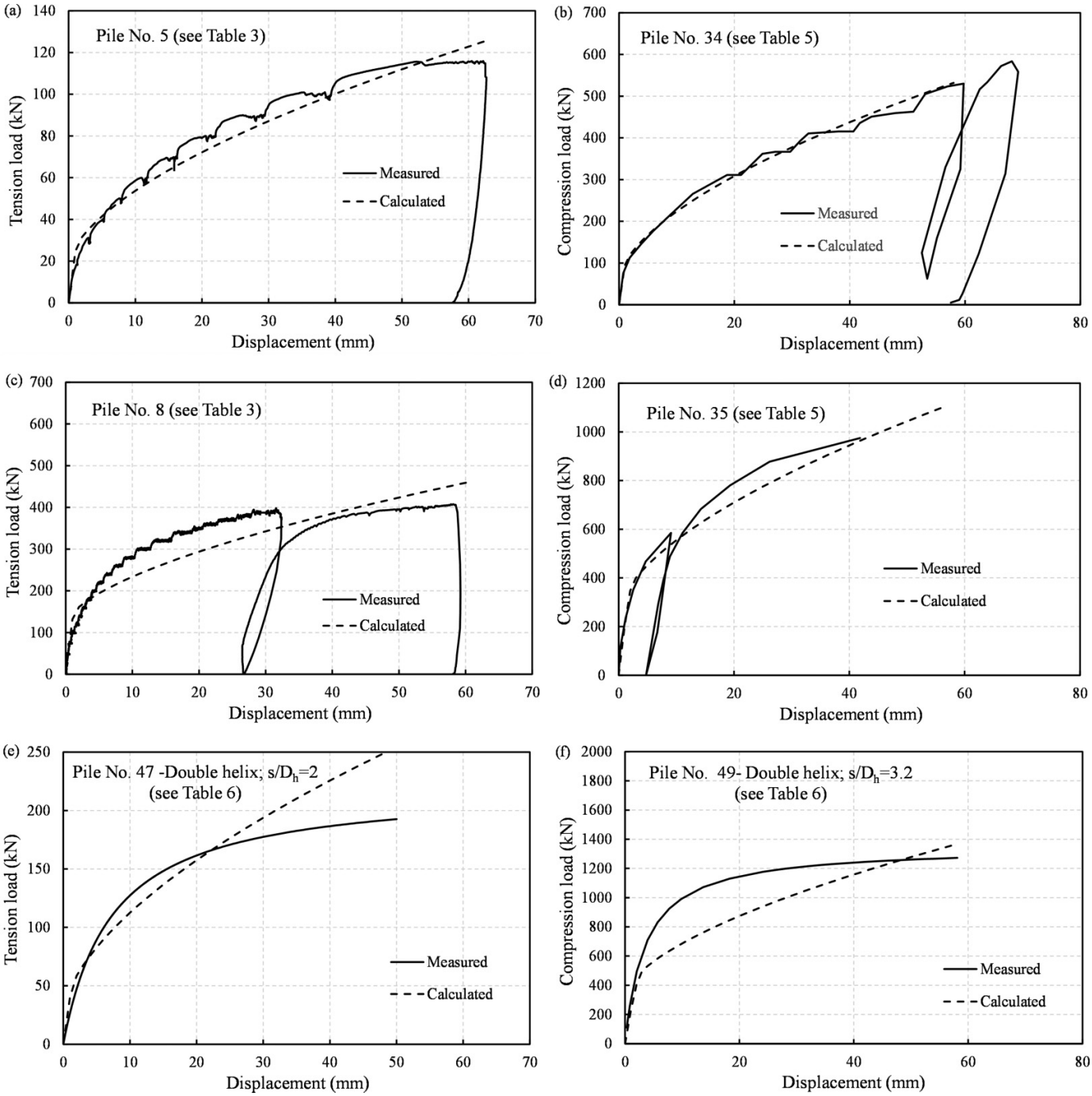

ized by the average q_c values within a distance of 1 D_h from the helix ($q/q_{c,avg}$) varies with the normalized helix movement (δ/D_h) raised to the power of approximately 0.6. The normalized displacement required to generate the peak shaft load (Q_{shaft}) is typically about 1% (API 2011). Combining both components of resistance then gives the following relationship between the total axial resistance (Q) and the pile displacement (δ), where Q_{shaft} is the ultimate shaft resistance:

$$(5) \quad Q = \left(\frac{\pi D_h^2}{4}\right)\left(kq_{c,avg}\left(\frac{\delta}{D_h}\right)^{0.6}\right) + Q_{shaft}; \delta > 0.01d$$

where the constant k is 0.6 in tension and 0.8 in compression (corresponding to respective best-fit $\alpha_{b0.1}$ values of 0.15 and 0.2).

The suitability of eq. 5 is examined on Fig. 7 which compares its predictions with the load-displacement response measured in typical tests where capacities ranged from 120 to 1200 kN. The tests considered include compression and tension loading of single helix piles (in Fig. 7*a*–7*d*) and double helix piles (in Fig. 7*e* and 7*f*). Details of all piles are provided in Tables 1, 2, 5 and 6. A reasonable match between the calculated and measured responses is seen on Fig. 7 confirming the

Table 5. Performance of UWASP-22 for database of single helix helical piles.

No	Pile name	Site name	Reference	Loading direction	L (m)	d (m)	D_h (m)	p (m)	$Q_{ult,\,c}$ (kN)	$Q_{ult,\,m}$ (kN)	$Q_{ult,\,m}/Q_{ult,\,c}$
21	S2P3	Alberta, Canada	Li and Deng (2019)	T	4.6	0.11	0.41	0.076	182.8	189	1.03
22	S2P1	Alberta, Canada	Li and Deng (2019)	T	2.4	0.07	0.31	0.076	104.3	88	0.84
23	S2P2	Alberta, Canada	Li and Deng (2019)	T	3.1	0.09	0.36	0.076	127.1	110	0.87
24	T9	Alberta, Canada	Tappenden (2007)	T	4.9	0.27	0.76	NR	2365.4	2025	0.86
25	T7	Ruth Lake, Canada	Tappenden (2007)	T	5.9	0.27	0.76	NR	866.2	800	0.92
26	PT	Blessington, Ireland	Gavin et al. (2014)	T	2.6	0.11	0.4	NR	303.6	240	0.79
27	P1T	Perth, Australia	SCPA	T	6.4	0.22	0.5	0.1	771.7	840	1.09
28	ST1	Perth airport, Australia	SCPA	T	6	0.32	0.6	0.1	601.9	554	0.92
29	ST1	Ellenbrook, Australia	SCPA	T	6	0.22	0.6	0.1	1219.7	1145	0.94
30	S2P3	Alberta, Canada	Li and Deng (2019)	C	4.6	0.11	0.41	0.076	162.1	135	0.83
31	S2P1	Alberta, Canada	Li and Deng (2019)	C	2.4	0.07	0.31	0.076	131.3	114	0.87
32	S2P1	Alberta, Canada	Li and Deng (2019)	C	3.1	0.09	0.36	0.076	160.9	143	0.89
33	C11	Ruth Lake, Canada	Tappenden (2007)	C	5.9	0.27	0.76	NR	1122.4	1094	0.97
34	PC	Blessington, Ireland	Gavin et al. (2014)	C	2.6	0.11	0.4	NR	415	420	1.01
35	P1C	Perth, Australia	SCPA	C	4.4	0.22	0.5	0.1	1004.3	1010	1.01
36	SC1	Port Hedland, Australia	SCPA	C	6	0.22	0.6	0.1	2227.8	2123	0.95
37	SC1	Perth airport, Australia	SCPA	C	6	0.32	0.6	0.1	743.6	715	0.96
38	SC1	Perth, Australia	SCPA	C	6	0.22	0.6	0.1	856.2	617	0.72
39	SC2	Perth, Australia	SCPA	C	8	0.22	0.6	0.1	1216	1027	0.84
40	SC1	Karrakatta, Ausralia	SCPA	C	4	0.17	0.48	0.1	252	265	1.05
41	SC2	Karrakatta, Australia	SCPA	C	4	0.17	0.48	0.1	359.2	345	0.96
42	SC1	Perth, Australia	SCPA	C	5.5	0.17	0.6	0.1	609.1	525	0.86
43	SC1	Ellenbrook, Australia	SCPA	C	6	0.22	0.6	0.1	1594.8	1399	0.88
NR	Not registered									μ	0.92
SCPA	Screw Piling Australia									**CoV**	0.09

Note: CoV = coefficient of variation.

Table 6. Performance of UWASP-22 for database of double helix helical piles.

No	Pile Name	Site Name	Reference	Loading direction	L (m)	d (m)	D_h (m)	s/D_h	p (m)	$Q_{ult,\,c}$ (kN)	$Q_{ult,m}$ (kN)	$Q_{ult,\,m}/Q_{ult,\,c}$
44	C4	Alberta, Canada	Li and Deng (2019)	C	5.0	0.22	0.36	1.5	0.356	457	470	1.03
45	C6	Alberta, Canada	Li and Deng (2019)	C	5.0	0.22	0.36	1.5	0.356	382	380	1.00
46	S2	Alberta, Canada	Li and Deng (2019)	C	5.2	0.22	0.36	3.0	0.356	600	636	1.06
47	2Ht	Shenton Park, Australia	This study	T	2.8	0.14	0.36	2.0	0.384	217	187	0.86
48	2Hc	Shenton Park, Australia	This study	C	2.8	0.14	0.38	2.0	0.384	284	230	0.81
49	C10	Alberta, Canada	Tappenden (2007)	C	9.3	0.24	0.45/0.5	3.2	0.460	1050	1240	1.18
50	T9	Ruth Lake, Canada	Tappenden (2007)	T	6.0	0.27	0.46	3.2	0.762	1520	1325	0.87
											μ	0.97
											CoV	0.13

Note: CoV = coefficient of variation.

similarity of the load-displacement response of a helix and shallow foundation. When an additional term is added in eq. 5 to represent a second helix, the approach is also seen on Fig. 7*e* and 7*f* to provide acceptable predictions of the load–displacement response. These piles had spacing ratios (s/D_h) of 2 and 3.2 and do not reveal strong evidence of interaction between the helices at typical working loads (i.e., less than half of the ultimate capacity), although the calculated resistance of the pile with $s/D_h = 2$ at very large displacements is higher than the measured resistance.

Table 7. Measured installation torques (T_m) vs. torques calculated using UWASP-22 combined with (1) Perko (2009) formulation ($T_{c,1}$) and (2) Tsuha and Aoki (2010) formulation ($T_{c,2}$).

No	Pile name	$Q_{t,c}$ (kN)	$T_{c,1}$ (kNm)	$T_{c,2}$ (kNm)	T_m (kNm)	$T_m/T_{c,1}$	$T_m/T_{c,2}$
1	1 H(c)oe	132	9	11	11	1.23	0.97
2	1 H(c)	142	9	12	11	1.15	0.9
3	1 H(b)	122	8	10	8	1	0.78
4	1 H(e)	128	8	10	9	1.04	0.86
5	1 H(a)	100	5	8	5	0.95	0.63
6	1 H(d)	100	5	8	6	1.13	0.81
7	1 H(f)	122	8	11	9	1.06	0.8
8	1 H(g)	350	19	28	20	1.02	0.7
10	1 H(c)	147	9	11	10	1.06	0.87
11	1 H(a)	122	6	9	7	1.06	0.76
12	1 H(b)	139	8	10	9	1.05	0.87
13	1 H(e)	127	8	10	10	1.24	0.98
14	1 H(d)	122	6	9	8	1.29	0.89
15	1 H(f)	141	9	10	9	1.04	0.86
16	1 H(a)	113	6	8	7	1.11	0.79
17	1 H(b)	127	8	9	10	1.29	1.07
18	1 H(d)	121	6	9	9	1.38	0.96
19	1 H(e)	127	8	10	12	1.48	1.18
21	S2P3	183	10	15	9	0.9	0.59
22	S2P1	104	4	7	3	0.82	0.45
23	S2P2	127	6	9	4	0.76	0.45
24	T9	2365	288	387	258	0.9	0.67
25	C11	866	112	140	85	0.76	0.61
26	SPT	304	16	28	19	1.17	0.67
27	P1T	772	78	93	100	1.28	1.08
28	ST1	602	92	96	103	1.12	1.07
29	ST1	1220	130	164	115	0.89	0.7
30	S2P3	183	10	15	7	0.7	0.46
31	S2P1	104	4	7	4	1.06	0.58
32	S2P2	127	6	9	5	0.91	0.54
33	C11	866	112	140	85	0.76	0.61
34	SPC	304	16	28	19	1.17	0.67
35	P1C	806	83	99	117	1.41	1.18
36	SC1	1780	183	239	250	1.36	1.05
37	SC1	602	92	96	115	1.25	1.2
38	SC1	650	69	88	95	1.38	1.08
39	SC2	940	100	126	115	1.15	0.91
40	SC1	196	16	22	25	1.57	1.15
41	SC2	274	23	30	25	1.1	0.82
42	SC3	503	39	64	45	1.17	0.71
43	SC1	1220	130	164	115	0.89	0.7
					μ	**1.10**	**0.82**
					CoV	**0.19**	**0.26**

Note: CoV = coefficient of variation.

Statistical assessments for single helix piles in the database revealed that the difference between the measured and calculated pile head displacement at 50% of the ultimate capacity (which is a typical working load) is typically less than 0.5% of the pile helix diameter ($0.005D_h$) and less than $0.01D_h$ for all cases.

7. Equation summary: UWASP-22

The foregoing analyses have indicated that the following equations, which are now referred to as the UWASP-22 method, may be used to estimate the axial capacity (Q_{ult}) of a typical helical pile in sand ($0.25 < d/D_h < 0.5$, $L/D_h > 5$, $s/D_h \geq 2$, $AR \leq 0.8$ and 0.075 m $< p <$ 0.2 m):

$$(6a) \quad Q_{shaft} = (q_{cs}/230)A_{shaft}$$

$$(6b) \quad Q_{hi} = 0.15q_{c,avg}\left(\pi D_{hi}^2/4\right) \text{ in tension at } \delta/D_{hi} = 0.1$$

$$(6c) \quad Q_{hi} = 0.20q_{c,avg}\left(\pi D_{hi}^2/4\right) \text{ in compression at } \delta/D_{hi} = 0.1$$

$$(6d) \quad Q_{ult} = Q_{shaft} + \sum Q_{hi} \text{ at } \frac{\delta}{D_{hi}} = 0.1 \text{ for } \frac{s}{D_h} \geq 2$$

where Q_{shaft} is the ultimate shaft friction, assumed to develop at $\delta/d = 0.01$, above the uppermost helix, q_{cs} is the average q_c along the pile shaft above the helix, Q_{hi} is the ultimate capacity of the i^{th} helix and $q_{c,avg}$ is the average q_c value within $1D_h$ of the helix in the direction of loading. The load displacement response can be estimated using eq. 5.

The mean and *CoV* of the ratio of measured capacities to capacities calculated using eq. 6d for the 50 pile tests considered in this paper (Tables 3, 4, 5 and 6) are 0.98 and 0.11. This *CoV* value is considerably smaller than for other design methods employed for bored and driven piles (Lehane et al. 2020; Doan and Lehane 2021). This high level of reliability reflects the suitability of the form of eqs. 5 and 6d, which are closely comparable to formulations employed successfully for footings on sand.

8. Torque prediction using the CPT

The approach described for axial capacity determination can be used in conjunction with existing torque-capacity relationships of Perko (2009) and Tsuha and Aoki (2010) to derive a simple means of estimating the torque required to install a helical pile.

Following the Perko (2009) approach for a pile with a single helix, the combination of eqs. 1a and 6d, adopting the tension capacity for the helix, gives the following relationship for torque (T), employing units of *kN* and *m* for force and length respectively:

$$(7) \quad T\,(kNm) = \left[(q_{cs}/230)A_{shaft} + 0.15q_{c,avg}\left(\pi D_{hi}^2/4\right)\right] \times 0.4d^{0.92}$$

The corresponding relationship for T obtained by combining eq. 6b with the proposal of Tsuha and Aoki (2010) is:

$$(8) \quad T = (q_{cs}/230)A_{shaft} \times 0.5d + \frac{0.15q_{c,avg}\pi D_h^2 d_c tan\left(\theta + \delta_r\right)}{8}$$

where $\theta = \tan^{-1}(p/\pi d_c)$ in degrees, $d_c = 2/3\ (D_h{}^3\text{-}d^3)/(D_h{}^2\text{-}d^2)$ and δ_r is the sand-steel interface friction angle (taken as 29°; Lehane et al. 2020).

Installation torques were calculated using the CPT data at the site of each test pile. Predicted final installation torques determined using the procedures of Perko (2009) and Tsuka and Aoki (2010) are labelled $T_{c,1}$ and $T_{c,2}$, respectively, and

these are compared with measured installation torques for single helix helical piles in Table 7.

As for axial capacity calculations, the predictive performance of eqs. 7 and 8 was expressed in terms of the mean (μ) and *CoV* of the ratios of measured to calculated torques (T_m/T_c). The average ratios of $T_m/T_{c,1}$ and $T_m/T_{c,2}$ of 1.10 and 0.82 with respective *CoVs* of 0.19 and 0.26 indicate that both equations provide a reasonable estimate of the installation torque. Equation 7 has a better average and lower CoV than eq. 8 and is therefore recommended. This equation only requires CPT resistance and shaft diameter as input data to determine *T*. Torque predictions for multi-helix piles were also evaluated using the same approach and, although predictions using eq. 7 were typically within 25% of measured values, further assessment with more pile cases is required.

9. Conclusions

An experimental study involving 20 displacement helical piles in medium dense and dense sand showed that the static capacities of the piles were relatively insensitive to the helix pitch (between 0.1 and 0.2 m), the shaft end condition (closed, open and tapered) and the AR (between 0.5 and 1.0). The capacity and stiffness were observed to vary with the CPT q_c value and were typically 25% higher for piles tested in compression than those subjected to tension. These trends are used in the development of a new simple empirical CPT based method, referred to as UWASP-22, applicable to typical helical pile geometries in sand. The method is shown to provide excellent predictions of capacity for 50 test piles at a range of well documented sites and for a variety of helical pile geometries. A simple formulation, based on an existing expression for shallow foundations, is also proposed that allows good predictions of the full load–displacement response using CPT data. In addition, the method is extended using the relationship between installation torque and capacity proposed by Perko (2009) to provide a means of estimating the installation torque using CPT data. As with any empirical method, UWASP-22 should be treated with caution for helical pile parameters that are outside those used in the method calibration.

List of symbols

AR	Advancement ratio
CoV	Coefficient of variation
CPT	Cone penetration test
d	Shaft pile diameter
d_c	Diameter of a circle corresponding to the helix surface area
D_h	Helix pile diameter
D_r	Relative density
F_r	CPT friction ratio
h	Distance from pile tip to top of helix
k	Constant empirical value for load-displacement prediction
K_0	In-situ lateral earth pressure coefficient
L	Pile embedded length
p	Pile helix pitch
q	Helix bearing pressure
$q_{b0.1}$	Base bearing pressure at a displacement of 10% of the pile diameter
q_c	CPT end resistance
Q_c	Calculated axial capacity
$q_{c,avg}$	Average q_c within a distance of D_h from helix
Q_{com}	Compression axial capacity
q_{cs}	Average q_c along the pile shaft above the helix
Q_m	Measured axial capacity (tension or compression)
q_s	Unit shaft friction
Q_{shaft}	Ultimate shaft resistance
Q_t	Tension axial capacity
Q_{ult}	Ultimate axial capacity (tension or compression)
Q	Total axial resistance for a pile head displacement δ
s	Spacing between helices
T	Installation torque
T_c	Calculated torque
$T_{c,1}$	Torque calculated according to Perko (2009)
$T_{c,2}$	Torque calculated using Tsuha and Aoki (2010)
T_m	Measured torque
V	Installation thrust
v	Vertical velocity of the pile during installation
$\alpha_{b0.1}$	Ratio of cone resistance to shaft friction base bearing pressure
$\alpha_{b0.1,c}$	Ratio of cone resistance to shaft friction base bearing pressure in compression
$\alpha_{b0.1,t}$	Ratio of cone resistance to shaft friction base bearing pressure in tension
β_c	Ratio of cone resistance to shaft friction
δ	Pile head displacement
δ_r	Interface friction angle
Δz_h	Vertical displacement of the helix after one helix revolution
θ	Helix angle
μ	Average
ω	Pile rotation rate during installation

Acknowledgements

This project received founding from the Engineering and Physical Science Research Council (EPSRC) (grant No. EP/N006054/1: Supergen Wind Hub Grand Challenges Project: Screw piles for wind energy. The authors would like to acknowledge Screw Piling Australia Pty. Ltd. (SCPA) for the load test data on helical piles. The first author acknowledges the support of the Australian Postgraduate Award at The University of Western Australia and BECAL-Paraguay.

Article information

History dates

Received: 25 April 2022
Accepted: 12 April 2023
Accepted manuscript online: 10 May 2023
Version of record online: 8 November 2023

Data availability

All data and models used during the study appear in the submitted article.

Author information

Author ORCIDs

Eduardo Bittar https://orcid.org/0000-0002-1377-7965
Barry M. Lehane https://orcid.org/0000-0003-0244-7423
Anthony Blake https://orcid.org/0000-0001-5718-7900
Benjamin Cerfontaine https://orcid.org/0000-0002-4833-9412

Author contributions

Conceptualization: EB, BML, AB
Data curation: EB, AB
Formal analysis: EB, BML
Funding acquisition: DR, DW
Investigation: EB, AB, SM
Methodology: EB, BML, SM
Project administration: EB, BML, AB, DW, BC
Resources: BML
Software: EB
Supervision: BML
Validation: EB, BML
Visualization: EB
Writing – original draft: EB, BML
Writing – review & editing: EB, BML, DW

Competing interests

No competing interests.

References

Alwalan, M.F., and El Naggar, M. H. 2021. Load-transfer mechanism of helical piles under compressive and impact loading. Int. J. Geomech. **21**(6): 04021082. doi:10.1061/(ASCE)GM.1943-5622.0002037.

API. 2011. Geotechnical and foundation design considerations for offshore structures. American Petroleum Institute, Washington, DC, USA.

Bittar, E., Lehane, B., Watson, P., and Deeks, A. 2020. Effect of cyclic history on the ageing of shaft friction of driven piles in sand. *In* Proceedings of the 4th International Symposium on Frontiers in Offshore Geotechnics, American Society of Civil Engineers, pp. 541–550.

Bittar, E.J., Lehane, B.M., Mahdavi, S., Blake, A.P., Richards, D.J., and White, D.J. 2022. A review of a CPT based axial capacity prediction of screw piles in sand. *Cone Penetration Testing 2022*. pp. 838–843.

Blake, A.P., Cerfontaine, B., Richards, D.J., Bittar, E.M., White, D.J., Lehane, B.M., et al. 2023. Field-tests to investigate the installation of screw piles in sand for offshore wind applications. J. Geotech. Geoenviron. Eng. ASCE(submitted).

Bradshaw, A.S., Zuelke, R., Hildebrandt, L., Robertson, T., and Mandujano, R. 2018. Physical modelling of a helical pile installed in sand under constant crowd. *In* Proceedings of the 1st International Symposium on Screw Piles for Energy Applications (ISSPEA). Dundee, UK. pp. 109–115.

Brown, M.J. 2019. Screw pile research at the University of Dundee. 1st International symposium on Screw Piles for Energy Applications. 1–13. doi:10.20933/100001123.

Burland, J. B., and Burbidge, M. C. 1985. Settlement of foundations on sand and gravel. Proceedings of the institution of Civil Engineers. **78(6)**: 1325–1381.

Bustamante, M., and Gianeselli, L. 1982. Pile bearing capacity prediction by means of static penetrometer CPT. *In* Proceedings of the 2nd European symposium on penetration testing. **Vol. 2**, Balkema, Amsterdam, the Netherlands. pp. 493–500.

Cerfontaine, B., Brown, M.J., Knappett, J.A., Davidson, C., Sharif, Y.U., Huisman, M., et al. 2021. Control of screw pile installation to optimise performance for offshore energy applications. Géotechnique, 1–16.

Chin, F.K. 1970. Estimation of the ultimate load of piles from tests not carried to failure. *In* Proc. 2nd Southeast Asian Conference on Soil Engineering, Singapore.

da Silva, D.M., and Tsuha, C. de H.C. 2021. Experimental investigation on the installation and loading performance of model-scale deep helical piles in very dense sand. Can. Geotech. J. **58**(9): 1379–1395. doi:10.1139/cgj-2020-0317.

Davidson, C., Brown, M.J., Cerfontaine, B., Al-Baghdadi, T., Knappett, J., Brennan, A., et al. 2020. Physical modelling to demonstrate the feasibility of screw piles for offshore jacket-supported wind energy structures. Géotechnique, 1–19.

Doan, L.V., and Lehane, B.M. 2021. CPT-Based Design Method for Axial Capacities of Drilled Shafts and Auger Cast-in-Place Piles. Journal of Geotechnical and Geoenvironmental Engineering, **147**(8): 04021077. doi:10.1061/(ASCE)GT.1943-5606.0002542.

Elsawy, M.K., El Naggar, M.H., Cerato, A., and Elgamal, A. 2019. Seismic performance of helical piles in dry sand from large-scale shaking table tests. Géotechnique, **69**(12): 1071–1085. doi:10.1680/jgeot.18.P.001.

EP/N006054/1. 2016. Screw piles for wind energy foundations. grant No. EP/N006054/1: Supergen Wind Hub Grand Challenges. Engineering and Physical Science Research Council (EPSRC).

Fateh, A.M.A., Eslami, A., and Fahimifar, A. 2017. Direct CPT and CPTu methods for determining bearing capacity of helical piles. Marine Georesources & Geotechnology, **35**(2): 193–207. Taylor & Francis. doi:10.1080/1064119X.2015.1133741.

Gavin, K., Doherty, P., and Tolooiyan, A. 2014. Field investigation of the axial resistance of helical piles in dense sand. Canadian Geotechnical Journal, **51**(11): 1343–1354. doi:10.1139/cgj-2012-0463.

Harnish, J.L. 2015. Helical Pile Installation Torque and Capacity Correlations. Ph.D. Thesis. The University of Western Ontario.

ICC-ES (International Code Council Evaluation Service). 2017. AC358 Helical Pile Systems and Devices. ICC-ES, Chicago, IL, USA. Available from https://icc-es.org/acceptance-criteria/ac358-2/ [accessed 24 October 2021].

Lehane, B., Liu, Z., Bittar, E., Nadim, F., Lacasse, S., Jardine, R., et al. 2020. A new "unified" CPT-based axial pile capacity design method for driven piles in sand. Proceedings of 4th International Symposium on Frontiers in Offshore Geotechnics(ISFOG 2020), pp. 462–477.

Lehane, B.M. 2012. Foundation capacity from the CPT. Keynote Lecture, Proc. 4th Int. Conf. on Geotechnical and Geophysical Site Characterisation, 1, ISC4, Recife, Brazil, pp. 63–82.

Lehane, B.M. 2019. EH Davis Memorial Lecture. CPT-based design of foundations. Australian Geomechanics Journal, **54**(4): 23–45.

Lehane, B.M., Ismail, M.A., and Fahey, M. 2004. Seasonal dependence of in situ test parameters in sand above the water table. Géotechnique, **54**(3): 215–218. doi:10.1680/geot.2004.54.3.215.

Lehane, B.M., Zania, V., Chow, S.H., and Jensen, M. 2022. Interpretation of centrifuge CPT data in normally consolidated silica and carbonate sands. Géotechnique, 1–10. doi:10.1680/jgeot.21.00177.

Li, A.Z., and Lehane, B.M. 2010. Embedded cantilever retaining walls in sand. Géotechnique, **60**(11): 813–823. doi:10.1680/geot.8.P.147.

Li, W., and Deng, L. 2019. Axial load tests and numerical modeling of single-helix piles in cohesive and cohesionless soils. Acta Geotechnica, **14**(2): 461–475. doi:10.1007/s11440-018-0669-y.

Lim, J. K. 2013. Time and scale effects on the shaft friction of displacement piles in sand. Ph.D. Thesis. The University of Western Australia.

Liu, Q.B., Lehane, B.M., and Tian, Y. 2020. Bearing capacity and stiffness of embedded circular footings on stiff-over-soft clay. Journal of Geotechnical and Geoenvironmental Engineering, **146**(11): 06020020. doi:10.1061/(ASCE)GT.1943-5606.0002393.

Lutenegger, A.J. 2009. Cylindrical shear or plate bearing? Uplift behavior of multi-helix screw anchors in clay. *In* Contemporary topics in deep foundations. pp. 456–463.

Lutenegger, A.J. 2013. Factors affecting installation torque and torque-to-capacity correlations for screw-piles and helical anchors. *In* Proceedings ofthe 1st International Geotechnical Symposium on Helical Foundations, Amherst, MA, USA, pp. 211–224.

Mayne, P.W., and Woeller, D.J. 2014. Generalized Direct CPT Method for Evaluating Footing Deformation Response and Capacity on Sands, Silts, and Clays. (1): 1983–1997.

Mitsch, M.P., and Clemence, S.P. 1985. Uplift Capacity of Helix Anchors in Sand. In Unknown Host Publication Title. American Society of Civil Engineers (ASCE), pp. 26–47.

Perko, H.A. 2009. Helical piles: a practical guide to design and installation. John Wiley & Sons.

Phoon, K.K., and Retief, J.V. 2016. Reliability of geotechnical structures in ISO2394. CRC Press.

Rao, S.N., Prasad, Y.V.S.N., and Shetty, M.D. 1991. The behaviour of model screw piles in cohesive soils. Soils and Foundations, **31**(2): 35–50. doi:10.3208/sandf1972.31.2_35.

Sakr, M 2012. Installation and performance characteristics of high capacity helical piles in cohesive soils. The Journal of the Deep Foundations Institute. **6(1)**: 41–57. doi:10.1179/dfi.2012.004.

Schneider, J.A., Fahey, M., and Lehane, B. 2008. Characterisation of an unsaturated sand deposit by in situ testing. *Edited by* A-B. Huang and P. W. Mayne. *In* Geotechnical and Geophysical Site Characterisation (Taipei, Taiwan ed., Vol. CD-ROM). (3rd International Symposium on Site Characterisation (ISC'3)). CRC Press/Balkema. pp. 633–638.

Sharif, Y.U., Brown, M., Ciantia, M.O., Cerfontaine, B., Davidson, C., Knappett, J., et al. 2020. Using DEM to create a CPT based method to estimate the installation requirements of rotary installed piles in sand. Canadian Geotechnical Journal, doi:10.1139/cgj-2020-0017.

Sharif, Y.U., Brown, M.J., Cerfontaine, B., Davidson, C., Ciantia, M.O., Knappett, J.A., et al. 2021a. Effects of screw pile installation on installation requirements and in-service performance using the discrete element method. Canadian Geotechnical Journal, **58**(9): 1334–1350. doi:10.1139/cgj-2020-0241.

Sharif, Y.U., Brown, M.J., Ciantia, M.O., Cerfontaine, B., Davidson, C., Knappett, J.A., and Ball, J.D. 2021b. Assessing single-helix screw pile geometry on offshore installation and axial capacity. Proceedings of the Institution of Civil Engineers –Geotechnical Engineering, pp. 1–18.

Spagnoli, G., and de Hollanda Cavalcanti Tsuha, C. 2020. A review on the behavior of helical piles as a potential offshore foundation system. Mar. Georesour. Geotechnol. **38**(9): 1013–1036.

Spagnoli, G., and Gavin, K. 2015. Helical piles as a novel foundation system for offshore piled facilities. *In* Proceedings of the Abu Dhabi International Petroleum Exhibition and Conference, Abu Dhabi, UAE, 9–12 November 2015.

Tappenden, K.M. 2007. Predicting the axial capacity of screw piles installed in western Canadian soils. M.Sc. dissertation. The University of Alberta, Edmonton.

Trofimenkov, J.G., and Mariupolskii, L.G. 1965, Screw piles used for mast and tower foundations. In Proceedings of Sixth International Conference on Soil Mechanics and Foundation Engineering, **Vol.11**, Montreal, Quebec, pp. 328–332.

Tsuha, C.H.C., and Aoki, N. 2010. Relationship between installation torque and uplift capacity of deep helical piles in sand. Can. Geotech. J. **47**(6): 635–647. doi:10.1139/T09-128.

Xu, X. 2007. Investigation of the end bearing performance of displacement piles in sand. Ph.D. thesis. The University of Western Australia.

Zhang, D.J.Y. 1999. Predicting capacity of helical screw piles in Alberta soils. M.Sc. dissertation. The University of Alberta, Edmonton.